

Review

Exploring aberration-corrected electron microscopy for compound semiconductors[†]David J. Smith^{1,*}, Toshihiro Aoki², John Mardinly², Lin Zhou^{1,3}
and Martha R. McCartney¹¹Department of Physics, Arizona State University, Tempe, AZ 85287-1504, USA, ²LeRoy Eyring Center for Solid State Science, Arizona State University, Tempe, AZ 85287-1704, USA and ³The Ames Laboratory, US Department of Energy, Iowa State University, Ames, IA 50011, USA

*To whom correspondence should be addressed. E-mail: david.smith@asu.edu

[†]This paper is dedicated to the memory of the late Akira Tonomura.

Abstract The development of aberration-corrected electron microscopes (ACEMs) has made it possible to resolve individual atomic columns ('dumbbells') with correct interatomic spacings in elemental and compound semiconductors. Thus, the latest generations of ACEMs should become powerful instruments for determining detailed structural arrangements at defects and interfaces in these materials. This paper provides a short overview of off-line ('software') and on-line ('hardware') ACEM techniques, with particular reference to characterization of elemental and compound semiconductors. Exploratory probe-corrected studies of ZnTe/InP and ZnTe/GaAs epitaxial heterostructures and interfacial defects are also described. Finally, some of the associated problems and future prospects are briefly discussed.

Keywords aberration-corrected electron microscopy, compound semiconductor, dumbbell imaging, polarity reversal

Received 4 February 2013, accepted 28 February 2013; online 27 March 2013

Introduction

The transmission electron microscope (TEM), with its many different configurations for imaging, diffraction and microanalysis, has become an indispensable tool for characterizing advanced materials. The TEM provides an unparalleled range of magnification, while the image resolution, aided by aberration correction, can nowadays surpass the one-Ångström level. In addition, the probe-corrected operating mode enables greatly enhanced current densities for rapid acquisition of elemental distributions with atomic-scale spatial resolution. Thus, the era of aberration-corrected electron microscopy (ACEM) offers many exciting possibilities for the discovery and exploitation of novel materials. The focus of this short review is on the emerging opportunities

for atomic ACEM imaging of elemental and compound semiconductors, especially for characterizing epitaxial heterostructures.

The diamond-cubic and zincblende semiconductors have lattice parameters that range from 0.357 nm (C) to 0.648 nm (CdTe), and it has been commonplace for many years to obtain lattice-fringe images from many of these materials in the major $\langle 110 \rangle$, $\langle 100 \rangle$ and $\langle 112 \rangle$ zone-axis projections. Crystal polarity was readily determined for both wurtzite and sphalerite materials by careful study of image appearance as a function of thickness and defocus [1,2], while genuine atomic imaging was achieved for elemental Si and Ge in $\langle 100 \rangle$, $\langle 111 \rangle$ and $\langle 113 \rangle$ orientations for particular operating conditions [3]. The projection most commonly used for

observing semiconductors is, however, the $\langle 110 \rangle$ orientation, since two sets of $\{111\}$ -type planes, which are most relevant to studying the generation of stacking defects, are then aligned edge-on to the beam direction. However, individual atomic columns, often referred to as ‘dumbbells’, cannot be separately resolved in this orientation unless the microscope resolution is sufficient to allow contributions to the final image from the $\{004\}$ -type reflections. Such demanding performance is beyond the capability of medium-voltage HREMs, although dumbbell-like images with ‘correct’ atomic-column spacings can be obtained at highly specific defocus settings in thicker crystal regions when the transmitted beam is weak and multiple electron scattering predominates [4].

The high-voltage, high-resolution electron microscope (HREM) has historically been considered the preferred tool for achieving better imaging performance, because the higher electron energy is associated with shorter electron wavelength [5]. Tonomura [6] fully appreciated that improved electrical and mechanical stabilities are essential for realization of the potential of higher-voltage operation, and remarkable lattice images clearly showing fringe spacings of finer than 0.5 \AA were obtained using his 1.0-MeV instrument, which was also equipped with a field-emission electron source for enhanced beam coherence [7]. In the present context of characterizing compound semiconductors, it is appropriate here to note that Ichinose *et al.* [8] were successful in obtaining atomic-resolution electron micrographs from 6H-SiC, using a 1.0-MeV microscope, so that individual Si and C atomic columns separated only by 1.09 \AA were clearly resolved. Atomic-column imaging for a twinned GaP crystal using a 1250-keV HREM has also been reported [9]. However, concerns about specimen damage caused by electron beam-irradiation effects, as well as the considerable expense of microscope purchase and upkeep, has seemingly constrained widespread deployment of similar high-voltage HREMs. Moreover, the concurrent emergence of aberration-correction techniques applicable to lower-voltage instruments has been a revolutionary development that has since completely altered the landscape for atomic-resolution electron microscopy

[10]. Some key aspects in the development of ACEMs are discussed in the following section.

Aspects of ACEM

The spherical aberration of circularly symmetric magnetic lenses is well known to limit the structural resolution of the TEM [11]. Three possible approaches to aberration correction were initially proposed based on time-varying fields, space charge or rotationally asymmetric electron-optical elements [11]. Many groups later experimented with different combinations of electrostatic and/or magnetic elements, using quadrupole–octopole or hexapole correctors to break the spherical symmetry [12], but no significant progress was achieved due primarily to the lack of any procedure for systematically adjusting the numerous mechanical components and electrical controls based solely on image appearance [13]. Other factors, including mechanical imperfections and electrical instabilities were additional handicaps [14]. Online microscope control [15], and automated diffractogram analysis [16], have since proved to be crucial steps along the path towards successful aberration correction [10]. The pioneering efforts of Tonomura *et al.* [17] in developing a field-emission electron gun (FEG) suitable for TEM operation have also been critical, since the enhanced spatial and temporal coherence provided by the FEG allow microscope information limits to be extended well beyond the interpretable (‘Scherzer’) resolution limit [18].

Aberration correction can be achieved offline using either focal-series reconstruction (FSR) or off-axis electron holography. The FSR approach led to the first observations of individual O atomic columns, using a 200-keV FEG TEM [19]. The greater information limits available with 300-keV operation later enabled improved visibility for elemental and compound semiconductors. For example, individual Ga and N atomic columns were observed on both sides of a cubic-GaN/2H-GaN interface [20], and individual C atomic columns separated only by 0.089 nm were also well resolved in $[110]$ -oriented diamond [21], as seen in Fig. 1. The core structure of a GaAs 30° partial dislocation was also investigated using the FSR approach, individual Ga–As

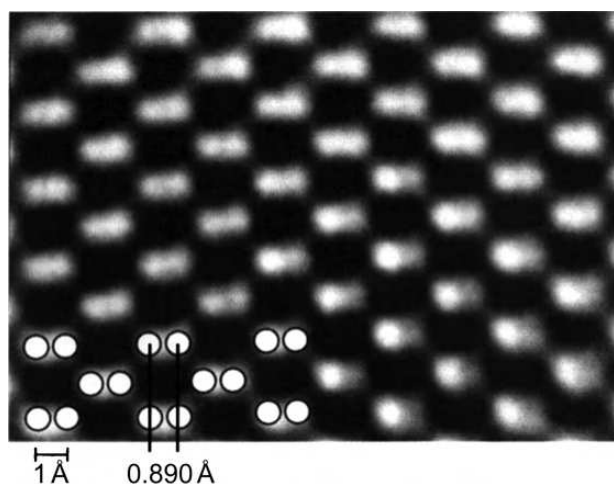


Fig. 1. A reconstructed phase image from a [110]-oriented diamond crystal after focal-series restoration showing individual atomic columns of carbon separated by 0.089 nm (courtesy of M.A. O’Keefe).

atomic-column positions being determined with an accuracy of ~ 0.01 nm [22].

Electron holography was initially proposed as a possible approach for surmounting the resolution limit imposed by spherical aberration [23]. The groundbreaking holography studies of Lichte and colleagues several decades later demonstrated for the first time the potential of the technique for overcoming the traditional aberration-limited resolution, and showed that individual Si atomic columns could be observed in reconstructed phase and amplitude images, as seen in Fig. 2 [24]. Further holography observations also showed that it was possible to differentiate in both phase and amplitude images between individual atomic columns in [110]-oriented GaAs, thereby enabling determination of the crystal polarity [25].

Both of these offline, software-based, approaches to aberration correction require accurate knowledge of critical lens parameters, which can be extracted from a tableau of diffractograms that are obtained using images of amorphous materials recorded with tilted illumination [26,27]. Moreover, it has been reported that compensation of lens aberrations before carrying out electron holography greatly simplifies the hologram reconstruction process and significantly improves the phase sensitivity [28,29]; this unexpected benefit could prove to be an important advantage for addressing the particular challenge of quantifying atomic-column occupancies at semiconductor defects and interfaces.

Online aberration correction involves inserting extra hardware, consisting of multipole elements, into the microscope column, as proposed by Scherzer [30]. A double-hexapole corrector unit with four additional (transfer) lenses immediately following the objective lens is commonly used on conventional image-corrected TEMs [31], whereas correctors composed of multiple quadrupole–octupole elements just preceding the objective lens are also used for probe-corrected scanning instruments [32]. The aberration-correction procedure in the TEM is based on the automated analysis of diffractogram tableaus, as described above, while the scanning TEM (STEM) approach employs shadow images, often termed Ronchigrams. In addition to correction of the spherical aberration (C_s) of the objective lens, both TEM and STEM online approaches compensate for other important imaging defects, including second- and third-order objective lens astigmatism as well as misalignment coma, thus significantly improving the quality as well as the quantity of the results that can be obtained. Exceptional stability of the deflector and corrector power supplies is required in either case (~ 0.1 ppm or better), and both procedures rely on the availability of a small area of amorphous material somewhere near the sample region of interest for correction purposes.

Dumbbell images for a [110]-oriented GaAs crystal were obtained during commissioning of the prototype 200-keV image-corrected TEM [31], and Si {110} atomic dumbbells were clearly resolved in some of the early high-angle annular-dark-field (HAADF) images obtained using a 100-keV probe-corrected STEM [33]. Further probe-corrected STEM results with dumbbell imaging have included observations of epitaxial $\text{CoSi}_2/\text{Si}(100)$ samples, which involved 7-fold- and 8-fold-coordinated Co interfacial atoms [34], and studies of partial and mixed dislocations in GaN [35]. More recently, dumbbell imaging with either [112]-oriented Ge (projected atomic-column separation of 0.082 nm) or [112]-oriented Si (projected atomic-column separation of 0.078 nm) has become the standard test for the evaluation and acceptance of probe-corrected STEMs. And there have been recent reports of dumbbell imaging with [114]-oriented Ge (projected atomic-column separation of 0.047 nm), albeit with

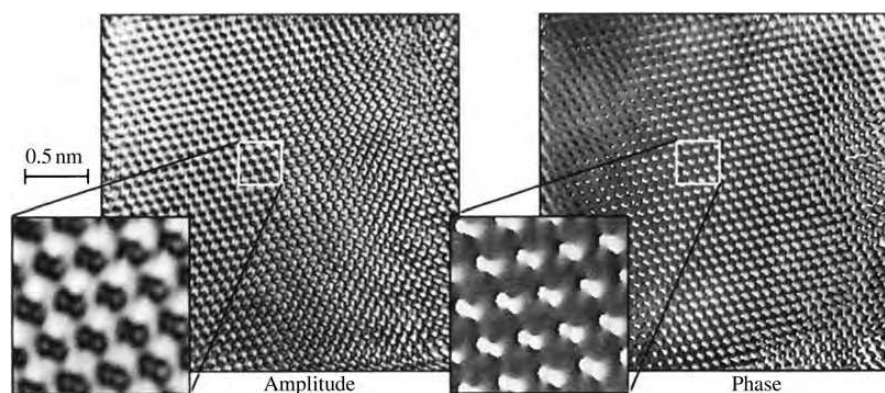


Fig. 2. Amplitude (left) and phase (right) images obtained after reconstruction of off-axis electron hologram, showing characteristic dumbbell appearance of individual Si atomic columns separated by 0.136 nm (courtesy of H. Lichte).

reduced contrast levels, using two different 300-keV probe-corrected STEMs [36,37].

Results

The ACEM studies reported recently in the literature seem mostly to have involved online (hardware) correction, with a heavy emphasis on probe correction. The HAADF or Z-incoherent contrast imaging mode of the STEM, which is strongly dependent on the atomic number of the atoms in the sample, preceded aberration correction, but the technique continues to be extensively used in probe-corrected instruments [38]. However, it should be appreciated that the STEM geometry permits considerable flexibility in the choice of the post-specimen detector configurations. Bright-field collection angles, which directly affect the image quality in terms of signal-to-noise ratio, can be greatly increased without impairment of resolution, because spatial coherence (beam divergence) is much less limiting in a probe-corrected instrument [39]. Moreover, annular-bright-field (ABF) imaging, which involves an annular detector placed within the incident cone of illumination, is capable of simultaneously imaging and differentiating between light and heavy atoms with reasonable contrast levels [40].

As an illustrative comparison of these various possibilities, Fig. 3 shows four different types of aberration-corrected STEM images recorded with a 200-keV JEOL-ARM200F, which were all taken from the same identical region of a specimen consisting of one-monolayer-thick InN/GaN multiple quantum

wells, which are of interest as near-ultraviolet light-emitting diodes [41]. Figure 3a presents the usual HAADF imaging geometry with detector collection angles in the range of ~ 90 – 170 mrad, while Fig. 3b is a medium-angle ADF image recorded with collection angles of ~ 20 – 60 mrad so that diffraction contrast is likely to have some influence on the overall image appearance in this case. The one-monolayer-thick InN layers (arrowed) are visible in both of these images, with brighter contrast along the lines corresponding to the In atomic columns. However, there is no apparent contrast corresponding to the positions of the low-Z atomic columns of nitrogen either in the InN active layer or in the GaN barrier layer. For comparison, Fig. 3c shows the corresponding BF image of the same area, recorded here with a collection angle spanning 0 – 22 mrad, and Fig. 3d shows the ABF image recorded with a collection angle of ~ 11 – 22 mrad. The crystal polarity is not apparent in Fig. 3c, but the separated black peaks visible in the ABF image show characteristic dumbbell contrast that readily allows identification of the crystal polarity, and all projected atomic-column positions are well resolved. Moreover, line profiles (not shown here) confirm that the In and Ga atomic columns have different intensity levels in both images. While the optimum conditions for fully quantitative studies using these various detector geometries have not yet been established, for example, by using systematic observations of wedge-shaped samples with matching image simulations, it seems that ABF imaging could be the preferred imaging mode for investigating samples that contain a combination of low-Z/high-Z elements.

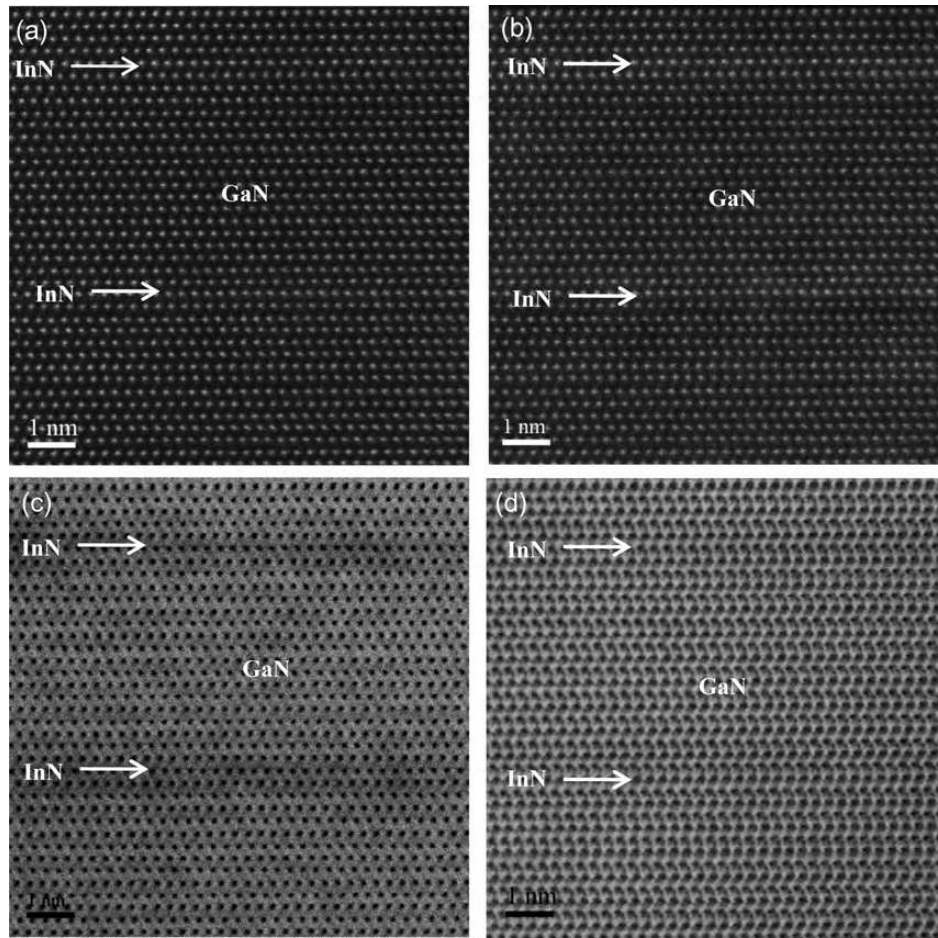


Fig. 3. Aberration-corrected STEM images showing InN/GaN multiple quantum wells recorded using four different detector configurations: (a) HAADF (90–170 mrad); (b) MAADF (20–60 mrad); (c) BF (0–22 mrad); and (d) ABF (11–22 mrad). The arrows indicate location of one-monolayer-thick InN quantum wells.

The microstructural characterization of semiconductor heterostructures, which continue to be of much interest for integrated electronic and optoelectronic applications, is an essential step towards achieving optimal epitaxial growth of high-quality materials. With a band gap of 2.27 eV at room temperature, ZnTe is a compound semiconductor of potential importance for multi-junction solar cell applications that can span a broad spectral range [42]. ZnTe ($a_0 = 0.6104$ nm) is closely lattice-matched to GaSb ($a_0 = 0.6096$ nm) and InAs ($a_0 = 0.6059$ nm), so that epitaxial growth of ZnTe on substrates of these materials should result in low defect densities. In contrast, there is greater lattice mismatch with InP ($a_0 = 0.5869$ nm) and GaAs ($a_0 = 0.5654$ nm), but these two materials are readily available as large-area, low-cost substrates. Thus, there is considerable interest and motivation for comparing and

possibly controlling defect formation processes associated with the growth of heteroepitaxial ZnTe on these different substrates [43]. Low-magnification images of ZnTe/InP samples previously showed high defect densities close to the heteroepitaxial interface, while higher-magnification images revealed that the interfacial defects for this mismatched system were primarily perfect 60° dislocations but also included a significant fraction ($\sim 13\%$) of Lomer edge dislocations [43].

Figure 4a and b compares two aberration-corrected (AC) STEM images that show a highly enlarged region of a ZnTe/InP (100) interface, which features an interfacial dislocation (arrowed) as well as a $\{111\}$ -type stacking fault (SF). The polarity of the InP and ZnTe layers on either side of the interface can be determined from the relative contrast levels of the dumbbells that are visible in

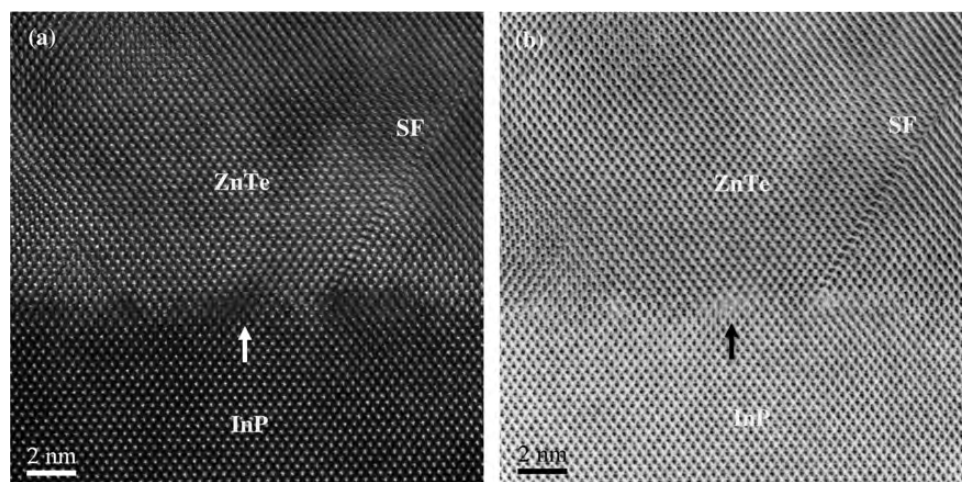


Fig. 4. AC-STEM images of ZnTe/InP(100) interface showing stacking fault (SF) and 60° perfect dislocation (arrowed): (a) HAADF (90–170 mrad); (b) BF (0–22 mrad).

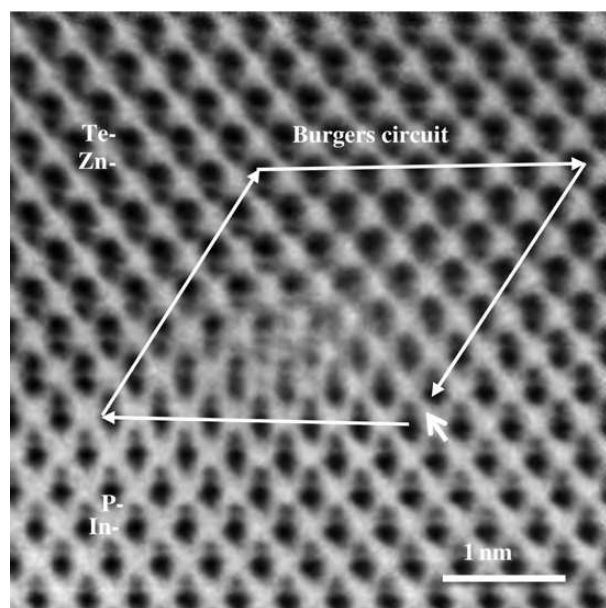


Fig. 5. An aberration-corrected BF STEM image of ZnTe/InP showing Burgers' circuit identifying 60° perfect dislocation. The polarity of In–P and Zn–Te dumbbells can be identified from relative atomic-column intensity.

both the HAADF (a) and BF (b) images. The Burgers' circuit analysis of the ZnTe/InP interfacial defect shown in Fig. 5 identifies a 60° perfect dislocation. All of the atomic columns in the bulk of both materials are clearly resolved in this image, although it does not seem possible by inspection to identify unambiguously the atomic arrangements at the core of the dislocation, perhaps because the defect structure may be disordered or dissociated along the beam direction.

Figure 6 compares HAADF and BF images of a Lomer edge dislocation occurring at the ZnTe/GaAs (100) interface. All the atomic columns in both materials are again well resolved in regions away from the defect, and it is also interesting to observe the apparent polarity reversal of the ZnTe epilayer relative to the orientation shown in Fig. 5 for growth on the InP substrate, which simply reflects observation in the orthogonal projection. Figure 7 shows intensity profiles along the two boxes indicated in Fig. 6a and b, and it is clear that the polarity of the Ga–As dumbbells in this orientation can be easily recognized for *both* detector configurations from the differences in their relative contrast levels, i.e. the heavier As columns ($Z=33$) are brighter than the lighter Ga columns ($Z=31$) in the HAADF image but darker in the BF image. However, the detailed atomic structure of the dislocation core is again not well resolved. Further observations are still required to determine whether this apparent disorder/dissociation is an intrinsic feature of these defects or whether sample preparation or beam-irradiation effects during preliminary observations have had some negative impact.

Concluding remarks

Great progress has recently been made towards aberration-corrected imaging of advanced materials, and the enormous potential of ACEM for determining the atomic configurations of defects and

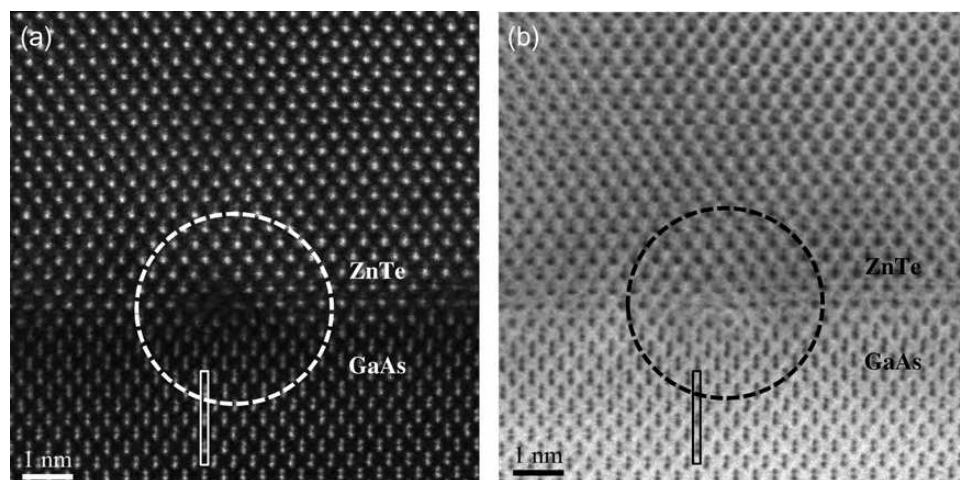


Fig. 6. AC-STEM images of ZnTe/GaAs(100) interface showing Lomer edge dislocation (circled): (a) HAADF (90–170 mrad); (b) BF (0–22 mrad). The boxes indicate regions used for intensity profiles shown in Fig. 6.

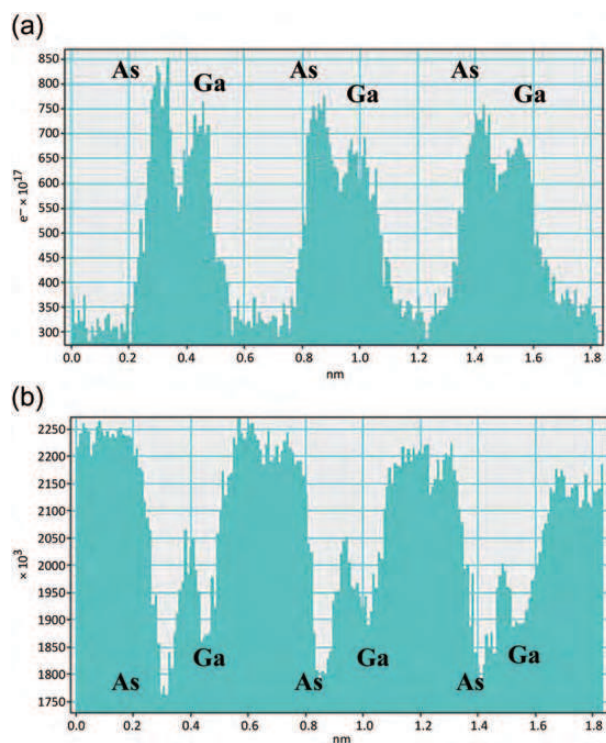


Fig. 7. Intensity profiles from boxes indicated on Fig. 6a and b, clearly showing Ga–As polarity in both cases.

interfaces in elemental and compound semiconductors should be self-evident. Realizing the full benefits of ACEM for quantitative defect determination will, however, require considerable extra time and effort in order to establish the preferred microscope operating conditions, since the optimal choice of imaging parameters, especially the C_s value and the

defocus setting, might be considered to be somewhat specimen-dependent. Image simulations are essential both for choosing microscope and specimen parameters and for confirming image interpretation when characterizing crystal defects. Amplitude contrast rather than phase contrast will actually dominate corrected TEM imaging for zero- C_s setting [44]. Moreover, it has been shown that imaging at a slightly overfocus condition with a small *negative* C_s value rather than zero offers more robust imaging conditions, as well as providing enhanced measurement precision approaching the picometer range [45]. Lattice defects in GaAs-based materials, with clear dumbbell imaging, were studied using negative- C_s imaging (NCSI), in combination with focal-series restoration to enhance overall signal quality [46].

No mention has so far been made of the possibilities of exploiting atomic-resolution elemental mapping, using the complementary techniques of energy-dispersive X-Ray spectroscopy and/or electron-energy-loss spectroscopy. The greatly enhanced current densities available in the probe-corrected STEM enable atomic-scale microanalysis with shorter acquisition times and improved sensitivity [47]. Moreover, the possibility of irreversible structural changes during analysis due to the intense incident probe can be greatly reduced, at least for some materials, by lower-energy observation [48]. Hence, there seem to be unexplored opportunities for investigating semiconductor defects

and especially compositional profiles across hetero-epitaxial interfaces, using either of these analytical methods, albeit while routinely monitoring for possible beam-induced changes during observation.

Acknowledgements

We acknowledge the use of facilities in the John M. Cowley Center for High Resolution Electron Microscopy at Arizona State University.

Funding

The acquisition of the JEM-ARM 200F at Arizona State University was supported by NSF Grant DMR-0821796.

References

- Glaisher R W, Spargo A E C, and Smith D J (1989) Systematic analysis of HREM imaging of wurtzite semiconductors. *Ultramicroscopy* **27**: 117–130.
- Glaisher R W, Spargo A E C, and Smith D J (1989) Systematic analysis of HREM imaging of sphalerite semiconductors. *Ultramicroscopy* **27**: 131–150.
- Bourret A, Rouviere J L, and Spendeler J (1988) Direct observation of atomic columns in semiconductors by HREM at 400 kV. *Phys. Stat. Sol. (A)* **107**: 481–501.
- Hutchison J L, Honda T, and Boyes E D (1986) Atomic imaging of semiconductors. *JEOL News* **24E**: 9–13.
- Phillipp F, Hoschen R, Osaki M, Mobus G, and Ruhle M (1994) New high-voltage atomic-resolution microscope approaching 1-Ångström point resolution installed in Stuttgart. *Ultramicroscopy* **56**: 1–10.
- Tonomura A (2003) Applications of 1 MV field-emission transmission electron microscope. *J. Electron Microsc.* **52**: 11–19.
- Kawasaki T, Yoshida T, Matsuda T, Oaskabe N, Tonomura A, Matsui I, and Kitazawa K (2000) Fine crystal lattice fringes observed using a transmission electron microscope with 1 MeV coherent electron waves. *Appl. Phys. Lett.* **76**: 1342–1344.
- Ichinose H, Sawada H, Takuma E, and Osaki M (1999) Atomic resolution HVEM and environmental noise. *J. Electron Microsc.* **48**: 887–891.
- Phillipp F (1996) Atomic resolution with a megavolt electron microscope. *Adv. Solid State Phys.* **35**: 257–276.
- Smith D J (2008) Development of aberration-corrected electron microscopy. *Microsc. Microanal.* **14**: 2–14.
- Scherzer O (1936) Über einige Fehler von Elektronenlinsen (Some defects of electron lenses). *Optik* **101**: 593–603.
- Hawkes P W and Kasper E (1989) *Principles of Electron Optics, Chap. 31* (Academic, London).
- Crewe A V (2004) Some Chicago aberrations. *Microsc. Microanal.* **10**: 414–419.
- Rose H (1994) Correction of aberrations, a promising means for improving the spatial and energy resolution of energy-filtering electron microscopes. *Ultramicroscopy* **56**: 11–25.
- Smith K C A (1982) On-line digital computer techniques in electron microscopy: general introduction. *J. Microsc.* **127**: 3–16.
- Krivanek O L and Mooney P A (1993) Applications of slow-scan CCD cameras in transmission electron microscopy. *Ultramicroscopy* **49**: 95–108.
- Tonomura A, Matsuda T, and Endo J (1979) Development of a field-emission electron-microscope. *J. Electron Microsc.* **28**: 1–11.
- van Dyck D, Lichte H, and vander Mast K D (1996) Sub-ångström structure characterisation: the Brite-Euram route towards one ångström. *Ultramicroscopy* **64**: 1–15.
- Coene W, Janssen G, Op De Beeck M, and van Dyck D (1992) Phase retrieval through focus variation for ultra-resolution in field-emission transmission electron microscopy. *Phys. Rev. Lett.* **69**: 3743–3746.
- Kisielowski C, Hetherington C J D, Wang Y C, Kilaas R, O'Keefe M A, and Thust A (2001) Imaging columns of the light elements carbon, nitrogen and oxygen with sub Ångström resolution. *Ultramicroscopy* **89**: 243–263.
- O'Keefe M A, Hetherington C J D, Wang Y C, Nelson E, Turner J, Kisielowski C, Malm J O, Mueller R, Ringnalda J, Pan M, and Thust A (2001) Sub-ångström high-resolution transmission electron microscopy. *Ultramicroscopy* **89**: 215–241.
- Xu X, Beckman S P, Specht P, Weber E R, Chrzan D C, Erni R P, Arslan I, Browning N D, Bleloch A R, and Kisielowski C (2005) Distortion and segregation in a dislocation core region at atomic resolution. *Phys. Rev. Lett.* **95**: 145501.
- Gabor D (1949) Microscopy by reconstructed wavefronts. *Proc. Roy. Soc. A* **197**: 454.
- Orchowski A, Rau W D, and Lichte H (1995) Electron holography surmounts resolution limit of electron microscopy. *Phys. Rev. Lett.* **74**: 399–402.
- Lehmann M and Lichte H (2005) Electron holographic material analysis at atomic dimensions. *Cryst. Res. Technol.* **40**: 149–160.
- Thust A, Overwijk M H F, Coene W M N, and Lentzen M (1996) Numerical correction of lens aberrations in phase-retrieval HRTEM. *Ultramicroscopy* **64**: 249–264.
- Barthel J and Thust A (2010) Aberration measurement in HRTEM: implementation and diagnostic use of numerical procedures for the highly precise recognition of diffractogram patterns. *Ultramicroscopy* **111**: 27–46.
- Geiger D, Lichte H, Linck M, and Lehmann M (2008) Electron holography with a C_s -corrected transmission electron microscope. *Microsc. Microanal.* **14**: 68–81.
- Lichte H, Linck M, Geiger D, and Lehmann M (2010) Aberration correction and electron holography. *Microsc. Microanal.* **16**: 434–440.
- Scherzer O (1947) Sparische und chromatische korrektur von elektronen-linsen. *Optik* **2**: 114–132.
- Haider M, Rose H, Uhlemann S, Schwan E, Kabius B, and Urban K (1998) A spherical-aberration-corrected 200 kV transmission electron microscope. *Ultramicroscopy* **75**: 53–60.
- Krivanek O L, Dellby N, and Lupini A (1999) Towards sub-Å electron beams. *Ultramicroscopy* **78**: 1–11.
- Dellby N, Krivanek O L, Nellist P D, Batson P E, and Lupini A R (2001) Progress in aberration-corrected scanning transmission electron microscopy. *J. Electron Microsc.* **50**: 177–185.
- Falke M, Falke U, Bleloch A L, Teichert S, Beddies G, and Hinneberg H J (2005) Real structure of the CoSi₂/Si(100) interface studied by dedicated aberration-corrected scanning transmission electron microscopy. *Appl. Phys. Lett.* **86**: 203103.
- Arslan I, Bleloch A L, Stach E A, and Browning N D (2005) Atomic and electronic structure of mixed and perfect dislocations in GaN. *Phys. Rev. Lett.* **94**: 025504.
- Erni R, Rossell M D, Kisielowski C, and Dahmen U (2009) Atomic-resolution imaging with a sub-50-pm electron probe. *Phys. Rev. Lett.* **102**: 096101.
- Takayanagi K, Kim S, Lee S, Oshima Y, Tanaka T, Tanishiro Y, Sawada H, Hosokawa F, Tomita T, Kaneyama T, and Kondo Y (2011) Electron microscopy at a sub-50 pm resolution. *J. Electron Microsc.* **60**: S239–S244.
- Pennycook S J (2012) Seeing the atoms more clearly: STEM imaging from the Crewe era to today. *Ultramicroscopy* **123**: 28–37.

- 39 Pennycook S J, Chisholm M F, Lupini A R, Varela M, van Benthem K, Borisevich A Y, Oxley M P, Luo W, and Pantelides S T (2008) Materials applications of aberration-corrected scanning transmission electron microscopy. *Adv. Imaging Electron Phys.* **153**: 327.
- 40 Findlay S D, Shibata N, Sawada H, Okunishi E, Kondo Y, Yamamota T, and Ikuhara Y (2009) Robust atomic resolution imaging of light elements using scanning transmission electron microscopy. *Appl. Phys. Lett.* **95**: 191913.
- 41 Dimakis E, Nikiforov A Y, Thomidis C, Zhou L, Smith D J, Abell J, Kao C K, and Moustakas T D (2008) Growth and properties of near-UV light emitting diodes based on InN/GaN quantum wells. *Phys. Stat. Sol. (A)* **205**: 1070–1073.
- 42 Wang S, Ding D, Liu X, Zhang X B, Smith D J, Furdyna J K, and Zhang Y H (2009) MBE growth of II-VI materials on GaSb substrates for photovoltaics applications. *J. Cryst. Growth* **311**: 2116–2119.
- 43 Ouyang L, Fan J, Wang S, Lu X, Zhang Y-H, Liu X, Furdyna J K, and Smith D J (2011) Microstructural characterization of thick ZnTe epilayers grown on GaSb, InAs, InP and GaAs (100) substrates. *J. Cryst. Growth* **330**: 30–34.
- 44 Lentzen M, Jahnke B, Jia C L, Thust A, Tillmann K, and Urban K (2002) High-resolution imaging with an aberration-corrected transmission electron microscope. *Ultramicroscopy* **92**: 233–242.
- 45 Jia C L, Houben L, Thust A, and Barthel J (2010) On the benefit of the negative-spherical-aberration imaging technique for quantitative HRTEM. *Ultramicroscopy* **110**: 500–505.
- 46 Tillmann K, Thust A, and Urban K (2004) Spherical aberration correction in tandem with exit-plane wave function reconstruction: interlocking tools for the atomic scale imaging of lattice defects in GaAs. *Microsc. Microanal.* **10**: 185–198.
- 47 Watanabe M, Kanno M, and Okunishi E (2010) Atomic-resolution elemental mapping by EELS and XEDS in aberration corrected STEM. *JEOL News* **45**: 8–15.
- 48 Krivanek O L, Chisholm M F, Nicolosi V, Pennycook T J, Corbin C J, Dellby N, Murfitt M F, Own C S, Szilagyi Z S, Oxley M P, Pantelides S T, and Pennycook S J (2010) Atom-by-atom structural and chemical analysis by annular-dark-field electron microscopy. *Nature* **464**: 571–574.